JGR Oceans

RESEARCH ARTICLE
10.1029/2026JC024071

# Linking Phytoplankton-Derived Dissolved and Particulate Carbon Production to Bacterial Metabolism Across Physical Dynamics in a Subtropical Marginal Sea

**Yao Liu[1,2], Jianhua Kang[3,4], Yibin Huang[1], Chengwen Xue[1], and Bangqin Huang[1,2]**

[1]State Key Laboratory of Marine Environmental Science, College of Ocean and Earth Sciences, Xiamen University, Xiamen, China, [2]National Observation and Research Station for the Taiwan Strait Marine Ecosystem, College of the Environment and Ecology, Xiamen University, Xiamen, China, [3]Third Institute of Oceanography, Ministry of Natural Resources, Xiamen, China, [4]College of Oceanography, Hohai University, Nanjing, China

**Abstract** Bacterial metabolism is a central driver of organic carbon transformation in the ocean, yet its coupling to distinct biogenic carbon pools produced by phytoplankton remains poorly constrained. We conducted seven cruises across diverse environmental gradients in the Taiwan Strait, a subtropical marginal sea of the Pacific, simultaneously quantifying bacterial metabolic rates alongside phytoplankton-derived particulate primary production (PPP) and dissolved primary production (DPP) to examine their relationships with bacterial metabolism. Phytoplankton-released DPP was generally insufficient to meet bacterial carbon demand (BCD), indicating substantial reliance on dissolved organic carbon regenerated from particulate organic matter through food-web processing. Bacterial production showed a stronger association with DPP, whereas bacterial respiration was more closely associated with PPP. Accordingly, bacterial growth efficiency (BGE) co-varied with the fraction of primary production released in the dissolved form, indicating systematic associations between phytoplankton carbon partitioning and bacterial metabolic balance. Bacteria-phytoplankton coupling further varied across distinct physical water masses. River-plume waters exhibited lower BGE and lower DPP fractions, whereas offshore oligotrophic waters exhibited higher BGE and higher DPP fractions. Upwelling and mixed waters displayed similar DPP fractions but differed in BGE and BCD, reflecting variability in environmental conditions and carbon supply dynamics. These findings provide observational constraints on bacteria-phytoplankton coupling and microbial carbon flow pathways in dynamic marginal seas.

**Plain Language Summary** Marine bacteria play a central role in the transformation of organic carbon produced by phytoplankton, yet their relationships with different forms of phytoplankton-derived carbon remain poorly understood. Using multiple cruises in the Taiwan Strait, a region influenced by rivers, upwelling, and water mixing, we measured bacterial activity alongside phytoplankton production of dissolved and particulate organic carbon. We found that dissolved carbon directly released by phytoplankton alone cannot meet the total bacterial carbon demand, which relies also on carbon regenerated from particulate matter. Fraction of bacterial assimilated carbon used for growth co-varied with the fraction of phytoplankton carbon released in the dissolved form. These patterns differed across water masses and were associated with variations in environmental conditions and carbon supply. Overall, our results highlight the links between physical variability, phytoplankton carbon production, and bacterial metabolism, improving our understanding of carbon cycling in dynamic marine systems.

**Key Points:**

- Concurrent measurements of bacterial metabolism and biogenic carbon production reveal bacteria-phytoplankton coupling across gradients
- Bacterial growth efficiency co-varies with the fraction of primary production released as dissolved organic carbon
- Physical forcing modulates bacteria-phytoplankton interactions, leading to distinct microbial carbon flow pathways among water masses

**Supporting Information:**

Supporting Information may be found in the online version of this article.

**Correspondence to:**

Y. Huang,
yibin.huang@xmu.edu.cn

**Citation:**

Liu, Y., Kang, J., Huang, Y., Xue, C., & Huang, B. (2026). Linking phytoplankton-derived dissolved and particulate carbon production to bacterial metabolism across physical dynamics in a subtropical marginal sea. *Journal of Geophysical Research: Oceans*, *131*, e2026JC024071. https://doi.org/10.1029/2026JC024071

Received 23 JAN 2026
Accepted 16 MAY 2026

**Author Contributions:**

**Conceptualization:** Yao Liu, Yibin Huang
**Funding acquisition:** Jianhua Kang, Yibin Huang, Bangqin Huang
**Investigation:** Jianhua Kang
**Methodology:** Yao Liu, Yibin Huang, Chengwen Xue
**Project administration:** Jianhua Kang, Bangqin Huang
**Visualization:** Yao Liu, Chengwen Xue
**Writing – original draft:** Yao Liu, Yibin Huang
**Writing – review & editing:** Jianhua Kang, Yibin Huang, Bangqin Huang



## 1. Introduction

The upper ocean plays a central role in the global carbon cycle, where phytoplankton primary production converts dissolved inorganic carbon into organic matter that fuels marine food webs (DeVries, 2022). Although only a small fraction of this newly fixed carbon is exported to the deep ocean, most is rapidly transformed and recycled within the euphotic zone through biological interactions (Azam & Malfatti, 2007; Siegel et al., 2023). Within this recycling-dominated system, heterotrophic bacteria are key regulators of organic carbon fate, assimilating carbon into biomass via bacterial production (BP) and remineralizing it back to $CO_2$ through bacterial respiration (BR), thereby controlling energy transfer, nutrient regeneration, and carbon retention in surface waters (Heneghan et al., 2024; Robinson, 2008). The balance between these processes, expressed as bacterial growth efficiency (BGE), determines whether organic carbon is retained in biomass or rapidly lost through respiration

(Del Giorgio & Cole, 1998); however, the mechanisms governing variability in bacterial metabolic demand and efficiency remain incompletely understood (Baumas et al., 2023).

At large spatial and temporal scales, bacterial metabolic activity broadly covaries with phytoplankton primary production, indicating that phytoplankton primary production serves as the principal organic carbon source supporting bacterial metabolism (Kim et al., 2022; Mühlenbruch et al., 2018). In many bacteria-phytoplankton coupling studies, primary production is primarily quantified as particulate primary production (PPP), as radiolabeled carbon ($^{13}C$ or $^{14}C$) fixed during photosynthesis is recovered on filters (GF/F > 0.7 μm or Nuclepore-PC > 0.2 μm) (Hama et al., 1983; Nielsen, 1952). As a result, these methods may underrepresent the fraction of photosynthetically fixed carbon that is released as dissolved organic carbon (DOC) during photosynthesis (Hansell & Orellana, 2021; Kang et al., 2024; Roshan & DeVries, 2017). PPP-focused estimates remain appropriate for addressing questions related to particulate carbon export, where sinking particles dominate carbon transfer to the ocean interior (Baumas et al., 2023). However, neglecting DOC production provides incomplete information for studies of microbial dynamics because phytoplankton-derived dissolved primary production (DPP) consists largely of low-molecular-weight compounds (e.g., simple sugars and amino acids) that are readily assimilated by bacteria and support microbial loop activity (Moran et al., 2022a, 2022b). By contrast, particulate organic carbon (POC) typically requires transformation through grazing, fragmentation, or enzymatic hydrolysis before becoming available to bacteria (Arnosti, 2011; Kujawinski, 2011). Growing evidence indicates that DPP can contribute a substantial and highly variable fraction of total primary production (TPP), commonly expressed as percent extracellular release (PER), ranging from ∼10% to more than 60% depending on ecosystem trophic status and environmental conditions (Boulion, 2021; Kang et al., 2024; Mühlenbruch et al., 2018; Poulton et al., 2016; Thornton, 2014).

Physical processes are also recognized as critical regulators of bacterial metabolism and bacteria-phytoplankton coupling in the ocean. Hydrodynamic forcing such as riverine inputs, upwelling, and deep convection processes can modify the physicochemical environment, thereby exerting direct controls on bacterial physiology and metabolic activity (Kim et al., 2017; Tamburini et al., 2013; Teira et al., 2016). Meanwhile, these physical processes can also indirectly influence bacterial metabolism by shaping both the magnitude of phytoplankton primary production and its partitioning between particulate and dissolved phases, which together determine the quantity and quality of organic carbon available to bacteria (Crump & Bowen, 2024; Dai et al., 2022). As a consequence, the fraction of primary production processed by bacteria varies widely along environmental and trophic gradients, ranging from ∼30% in highly productive systems (e.g., coastal upwelling regions or river-influenced waters) to values approaching or even exceeding 100% in low-productivity or recycling-dominated environments (e.g., oligotrophic open ocean gyres), leading to fundamentally different carbon flow pathways and energy transfer efficiencies (Azam, 1998; Del Giorgio et al., 1997; Ducklow, 2000; Huang et al., 2022). Resolving how bacterial metabolism couples to phytoplankton production under complex hydrodynamic conditions is therefore essential for understanding the spatial heterogeneity of upper-ocean carbon cycling and its implications for ecosystem functioning and carbon sequestration.

To address these gaps, we conducted seven cruises in the highly dynamic subtropical Taiwan Strait, simultaneously quantifying bacterial carbon metabolism—including BP and BR—together with phytoplankton primary production partitioned into dissolved and particulate carbon pools. The Taiwan Strait is located in the subtropical marginal sea of the Pacific Ocean and is characterized by the coexistence of major river plume systems and monsoon-driven upwelling, generating pronounced hydrodynamic variability and strong water mass heterogeneity (Chen, Yan, & Jiang, 2014; Zhong et al., 2020). These conditions make the region an ideal natural laboratory for investigating how physical forcing and production of distinct biogenic carbon jointly regulate bacteria-phytoplankton coupling and carbon flow pathways.

Our results show that although DPP alone cannot fully satisfy bacterial metabolic demand, BGE shows systematic co-variation with the partitioning of primary production between dissolved and particulate carbon pools. In addition, these relationships vary across distinct water masses, reflecting differences in environmental conditions and carbon supply dynamics. Overall, our study provides insights for linking partitioning of primary production between dissolved and particulate carbon pools, and physical variability to bacterial metabolism. It also offers key observational constraints for assessing regional carbon budgets and biological pump efficiency.

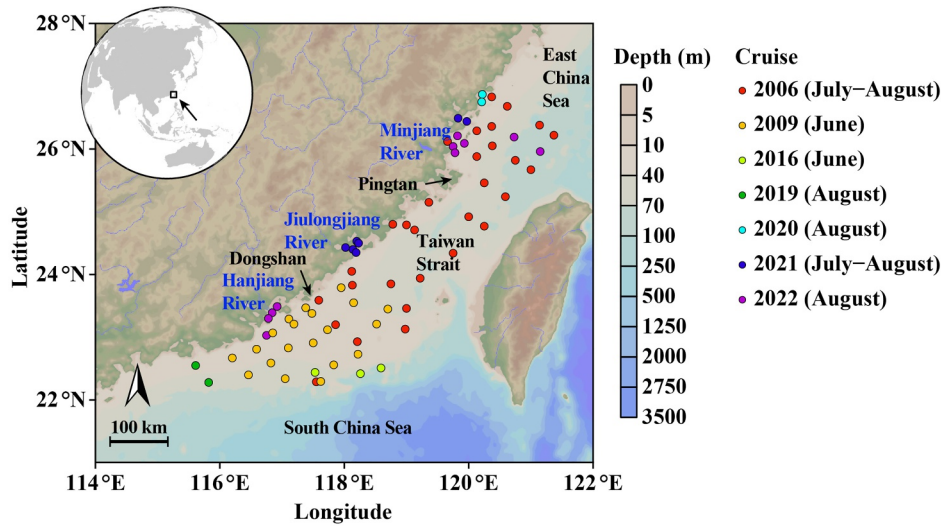


**Figure 1.** Spatial distribution of sampling stations across the Taiwan Strait during multiple research cruises conducted under the southwest monsoon.

## 2. Materials and Methods

### 2.1. Study Area and Data Sources

The Taiwan Strait, located between the southeastern coast of mainland China and Taiwan Island, connects the East China Sea to the South China Sea and serves as a major pathway for water mass exchange between these two marginal seas (Figure 1). Owing to its narrow geometry and complex bathymetry, the strait is characterized by vigorous hydrodynamic activity and strong water column mixing, resulting in pronounced spatial and temporal heterogeneity. Regional physical and biogeochemical processes are jointly regulated by the Asian monsoon system and terrestrial inputs. The northeast monsoon dominates during winter, whereas the southwest monsoon prevails in summer and is associated with pronounced coastal upwelling (Tang et al., 2002; Zhang, 2021). In addition, major rivers—including the Minjiang, Jiulongjiang, and Hanjiang Rivers—continuously discharge freshwater and nutrients into the strait, further shaping water mass structure, nutrient regimes, and ecosystem dynamics with strong seasonal variability (Chen, Yan, & Jiang, 2014; Zhong et al., 2020). Against the backdrop of climate warming and intensifying anthropogenic pressures, the Taiwan Strait has exhibited increasing sensitivity to environmental change, including rising sea surface temperatures and coastal eutrophication (Chen et al., 2024; Lee et al., 2021), making it an important natural laboratory for investigating climate-driven ecological responses.

The data used in this study is based on in situ observations collected during seven cruises conducted in the Taiwan Strait (115.61°E–121.37°E, 21.24°N–26.87°N) between 2006 and 2022 (Figure 1), encompassing a total of 74 sampling stations. All cruises were carried out during the summer southwest monsoon period, when diverse hydrodynamic regimes—including coastal upwelling, river plume influence, and intense water mass mixing—coexist across the region. At each station, vertical profiles of temperature and salinity were measured using a Sea-Bird SBE 9/11 or SBE 9/17 Plus conductivity-temperature-depth system (Sea-Bird Electronics, USA). Photosynthetically active radiation (PAR) profiles were obtained using an integrated radiometer sensor (Biospherical Instruments, USA). Based on the attenuation of PAR, six discrete depths were selected within the euphotic zone, corresponding to 100%, 50%, 30%, 10%, 5%, and 1% of surface PAR. Seawater samples were collected at these depths using Niskin bottles for subsequent chemical analyses and biological rate measurements (Figure S1 in Supporting Information S1). This PAR-based sampling strategy is commonly used in primary production studies to resolve vertical gradients in light availability and to facilitate accurate simulation of in situ light conditions during incubation experiments (Cloern et al., 2014; Liu et al., 2024). Bacterial metabolism and associated environmental parameters were measured at the same depths to ensure consistency with the light-dependent structure of phytoplankton production.

The part of observational data used in this study has been previously reported by Kang et al. (2024), who primarily focused on the spatial variability of DPP in the Taiwan Strait. Here, we further integrate and reanalyze these data

**Table 1**
*List of Abbreviations Used in This Study*

| Abbreviation | Full name | Unit |
|---|---|---|
| BP | Bacterial production | mg C $m^{-3}$ $d^{-1}$ |
| BR | Bacterial respiration | mg C $m^{-3}$ $d^{-1}$ |
| BCD | Bacterial carbon demand | mg C $m^{-3}$ $d^{-1}$ |
| BGE | Bacterial growth efficiency | % |
| DPP | Dissolved primary production | mg C $m^{-3}$ $d^{-1}$ |
| PPP | Particulate primary production | mg C $m^{-3}$ $d^{-1}$ |
| TPP | Total primary production | mg C $m^{-3}$ $d^{-1}$ |
| PER | Percent extracellular release of DPP | % |

sets with bacterial metabolic measurements, with a specific emphasis on bacteria-phytoplankton coupling and its regulating mechanisms. In addition, we applied a refined water mass classification and clustering approach to resolve contrasts in bacteria-phytoplankton coupling and carbon flow pathways among distinct hydrodynamic regimes. All data used in this study are publicly available in Liu et al. (2026). A complete list of abbreviations used in this study is provided in Table 1.

### 2.2. Bacterial Metabolism

Bacterial metabolism was quantified through simultaneous measurements of BP and BR. BP was determined using the $^{3}$H-leucine incorporation method (Kirchman, 2001). For each sample, seawater was dispensed into three sterile 50-mL centrifuge tubes, each containing 20 mL of seawater. One tube served as a killed control and was fixed immediately prior to incubation by adding 1 mL of formaldehyde. Radiolabeled $^{3}$H-leucine was added to all tubes to a final concentration of 20 nmol $L^{-1}$, a level generally considered sufficient to saturate incorporation rates in aquatic bacterial communities, thereby minimizing substrate limitation (Kirchman, 2001). Samples were incubated in the dark at in situ temperature for 1 hr, after which incubations were terminated by the addition of 1 mL formaldehyde. This short incubation time ensures measurements remain within the linear phase of substrate incorporation and minimizes potential bottle effects or physiological shifts. Similar $^{3}$H-leucine concentrations and incubation times have been widely used in previous studies conducted in the Taiwan Strait and adjacent regions (Chen, Huang, et al., 2014; Liu et al., 2025), supporting the comparability of our measurements with regional observations. After incubation, the samples were filtered under low vacuum pressure (<0.03 MPa) onto 0.2-μm polycarbonate filters (Millipore, USA). Radioactivity retained on the filters was measured using a Tri-Carb 3110 TR liquid scintillation counter (PerkinElmer, USA), and leucine incorporation rates were calculated after correction for killed controls. Leucine incorporation rates were converted to carbon units using a leucine-to-carbon conversion factor of 1.5 kg C mol leucine$^{-1}$, consistent with values recommended for the Taiwan Strait in previous regional studies (Kang et al., 2024).

BR was measured using a prefiltered bottle incubation approach (Robinson, 2008). Seawater samples were gently filtered under low vacuum pressure (<0.03 MPa) through 0.8-μm polycarbonate filters (Millipore, USA) to remove phytoplankton and grazers. The filtrate was transferred via silicone tubing into 100-mL biological oxygen demand bottles, allowing overflow volumes exceeding 300 mL to ensure complete removal of air bubbles. At each station, three initial bottles and three dark bottles were prepared. Dissolved oxygen concentrations in the initial bottles were immediately fixed using Winkler reagents (3 mol $L^{-1}$ $MnCl_2$ and 4 mol $L^{-1}$ NaI/8 mol $L^{-1}$ NaOH) and determined by high-precision potentiometric titration (Metrohm 848 Titrino Plus, Switzerland). Dark bottles were incubated for 24 hr in temperature-controlled darkened on-deck seawater baths, after which dissolved oxygen was measured following the same procedure. BR was calculated from the decrease in dissolved oxygen concentration during incubation and converted to carbon units using a respiratory quotient of 1 mol C per mol $O_2$ consumed (Robinson, 2008).

Total bacterial carbon demand (BCD) was calculated as the sum of BP and BR (BP + BR), while bacterial growth efficiency (BGE) was expressed as the percentage ratio of BP to BCD (BP/BCD × 100%) (Table 1). Even though 24 hr incubations are commonly applied to obtain measurable oxygen consumption rates (Robinson, 2008), we acknowledge that BP and BR were measured over different timescales and may not represent identical physiological states. However, our analysis focuses on relative spatial variations rather than absolute rate estimates, thereby reducing potential biases associated with differences in incubation duration. We also note that prefiltration through a 0.8-μm filter may exclude a fraction of particle-associated bacteria, potentially leading to an underestimation of BR and a corresponding overestimation of BGE. Nevertheless, previous studies have verified that particle-attached bacteria generally represent less than 15% of the total bacterial community even in particle-rich plumes or coastal regions, and an even smaller fraction offshore (Del Giorgio et al., 2011; Guo et al., 2022). Our results also indicate that despite this potential bias, BGE in plume and coastal regions remains lower than that in offshore environments. Therefore, this methodological limitation is unlikely to affect our conclusion regarding the relatively low BGE observed in plume waters, which also exhibit lower PER (see Results Section 3.2).

### 2.3. Phytoplankton Primary Production Partitioned Into Particulate and Dissolved Carbon Pools

Phytoplankton primary production was quantified using the $^{14}C$ tracer technique following the protocols described in Kang et al. (2024), with explicit partitioning between particulate and dissolved carbon pools. At each sampling depth, 750 mL of seawater was collected and distributed into three 250-mL polycarbonate bottles. Each bottle was amended with 740 kBq $NaH^{14}CO_3$ and incubated for 24 hr under in situ temperature conditions. Two bottles were incubated under ambient light, with neutral density screens applied to simulate in situ light conditions by adjusting light transmittance to match the PAR levels at each sampling depth, while one completely dark bottle was used to correct for non-photosynthetic carbon fixation. At the end of incubation, the samples were gently filtered under low vacuum pressure (<0.03 MPa) through 0.2-μm polycarbonate filters (Millipore, USA). The material retained on the filters was used to quantify PPP while the filtrate was collected for the determination of DPP. Filters were placed into scintillation vials and acidified with 1 mL of 0.1 mol $mL^{-1}$ HCl for 15 min to remove inorganic carbon. Filtrates were transferred into separate scintillation vials, acidified to pH = 2 with HCl, and purged with nitrogen gas for 24 hr to eliminate residual inorganic $^{14}C$. Following acidification and degassing, a scintillation cocktail was added to all vials, and radioactivity was measured using a Tri-Carb 3110 TR liquid scintillation counter (PerkinElmer, USA). Carbon fixation rates were calculated from the measured radioactivity following the standard $^{14}C$ assimilation approach (Equation 1; Peterson, 1980):

$$PP = \frac{1.05 \times (DPM_{light} - DPM_{dark}) \times DIC}{DPM_{total} \times t} \quad (1)$$

where PP is the carbon fixation rates; the factor 1.05 is a correction factor for the discrimination between $^{12}C$ and $^{14}C$; $DPM_{light}$ is the radioactivity measured in the particulate or dissolved fraction of the light bottle; $DPM_{dark}$ is the corresponding radioactivity measured in the dark bottle; $DPM_{total}$ is the total activity of added $NaH^{14}CO_3$; DIC is the ambient dissolved inorganic carbon concentration; and $t$ is the incubation time. PPP and DPP were calculated separately from the radioactivity retained on the filter and in the filtrate, respectively. Total primary production was defined as the sum of PPP and DPP (PPP + DPP), and the PER of DPP (PER) was computed as DPP/TPP × 100% (Table 1).

### 2.4. Chlorophyll-*a* and Nutrient Measurements

Chlorophyll-*a* concentrations were determined using a size-fractionated filtration approach. For each sample, 1 L of seawater was sequentially filtered under low vacuum pressure (<0.03 MPa) through 20-μm, 2-μm, and 0.2-μm filters (Whatman, UK), separating phytoplankton into microphytoplankton (>20 μm), nanophytoplankton (2–20 μm), and picophytoplankton (0.2–2 μm) size classes. Each filter was extracted in 10 mL of 90% acetone at −20°C for 24 hr, and chlorophyll-*a* concentrations were measured using a Turner Designs fluorometer (Model 10-AU-005, USA) (Yentsch & Menzel, 1963). Total chlorophyll-*a* was calculated as the sum of the three size fractions. Dissolved inorganic nutrients, including nitrate, phosphate, and silicate, were measured using a Flow AutoAnalyzer (QUAATRO, BRAN + LUEBBE, Germany) following standard colorimetric procedures (Grasshoff et al., 1999).

### 2.5. Water Mass Classification

In the Taiwan Strait, hydrographic structure and biogeochemical processes are primarily regulated by the East Asian monsoon system. Many previous studies partitioned observations according to monsoon phases, typically contrasting the northeast and southwest monsoon regimes (Lee et al., 2021; Liu et al., 2003; Zhong et al., 2020). Because all cruises analyzed in this study were conducted during the southwest monsoon season (Figure 1), we treated observations from different years as a unified data set and focused on resolving spatial heterogeneity among distinct water masses within the southwest monsoon regime.

To disentangle the effects of hydrodynamic structure on bacteria-phytoplankton coupling and microbial-mediated carbon flow pathways, water masses in the Taiwan Strait were classified using a multivariate clustering approach based on combined observations from all cruises. For each station, sea surface temperature, sea surface salinity, sea surface chlorophyll-*a* concentration, and distance from the coast were selected as key classification variables. Prior to analysis, chlorophyll-*a* and distance from the coast were log-transformed to improve normality, and all variables were standardized to remove scale dependence. Principal component analysis followed by hierarchical

clustering using Ward's minimum variance method was performed using the FactoMineR package (Lê et al., 2008). The resulting clusters were mapped onto spatial distributions and evaluated against regional hydrographic patterns and climatological satellite observations to ensure that the identified water masses were physically and biogeochemically coherent.

### 2.6. Statistical Analysis

All statistical analyses and visualizations were performed in *R* (version 4.2.0). To facilitate comparison across stations, all depth-resolved measurements (BP, BR, DPP, PPP, and associated environmental parameters) were vertically integrated over the euphotic zone using the trapezoidal method, and then normalized by the euphotic depth, yielding depth-averaged values. Differences in water column structure, environmental variables, primary production, bacterial metabolism, and carbon flow characteristics among water masses were assessed using Kruskal-Wallis nonparametric tests, with significance defined as $p < 0.05$.

To examine the coupling between bacterial metabolism and phytoplankton primary production and to identify their dominant drivers, Spearman rank correlation analyses were applied to evaluate associations among temperature, salinity, nutrient availability, phytoplankton size structure, primary production, and bacterial metabolic rates. Partial least squares path modeling was conducted using the plspm package (Sanchez, 2013) to explore the cascading relationships across multiple variables. Measured variables were first assigned to four latent constructs in the model: nutrient availability represented by nitrate, phosphate, silicate, and the N:P ratio; phytoplankton community structure characterized by chlorophyll-*a* concentrations of three size classes; primary production partitioning reflected by DPP, PPP, and PER; and bacterial carbon metabolism represented by BP, BR, and BGE. Weight factors were then calculated for each variable to show its relative contribution to the associated latent construct, with both the magnitude and sign of weights reflecting its importance and directional effect within the construct. Standardized path coefficients were ultimately computed to assess the direction, strength and significance of direct and indirect effects among latent constructs, with positive/negative coefficients indicating positive/negative relationships, respectively. Model performance was assessed using the coefficient of determination ($R^2$) and goodness of fit (GOF), with a GOF value approaching 0.7 indicating a satisfactory model fit.

## 3. Results

### 3.1. Water-Mass-Based Delineation of Ecological Regimes

Based on a multivariate clustering analysis integrating physical and biological variables (see Method Section 2.5), our sampling stations in the Taiwan Strait were classified into four representative ecological regimes (Figure 2a). Comparisons with climatological satellite observations indicate that these regimes exhibit overall stable spatial distributions and temporal persistence, and their hydrographic and biological characteristics are highly consistent with previously reported water mass structures in the region (Figure S2 in Supporting Information S1).

Nearshore stations strongly influenced by discharge from the Minjiang, Jiulongjiang, and Hanjiang Rivers were classified as the plume region (red dots, n = 18), with low salinity (generally <30), high nutrient and chlorophyll-*a* concentrations, and phytoplankton dominated by micro- and nanophytoplankton (Figures 2b–2i; Table S1 in Supporting Information S1). In contrast, oligotrophic waters (blue dots, n = 21) were distributed along a cross-shelf gradient from north to south, reflecting their offshore location rather than a single spatial cluster. These waters were characterized by high salinity, the lowest nutrient concentrations, and low chlorophyll-*a* levels (generally <0.5 mg $m^{-3}$), with phytoplankton assemblages dominated by picophytoplankton (Figures 2b–2i; Table S1 in Supporting Information S1). Upwelling stations (green dots, n = 14) were located in three regions—the Taiwan Bank, Dongshan coast, and waters adjacent to Pingtan, consistent with multiple upwelling systems driven by the southwest monsoon and local topography (Figure S2 in Supporting Information S1). Despite their separation, these stations shared similar hydrographic and biogeochemical characteristics, including temperatures ~1°C–2°C lower than the surrounding waters, relatively high salinity (~34), and elevated nutrient and chlorophyll-*a* levels (Figures 2b–2i; Table S1 in Supporting Information S1). The remaining stations were classified as a mixed water region, as they did not exhibit a single dominant hydrographic or biological characteristic. These stations (orange dots, n = 21) were primarily located in transition zones between the plume, upwelling, and oligotrophic waters, and displayed relatively high temperature and salinity, along with moderately elevated nutrient and chlorophyll-*a* levels, reflecting the combined influence of multiple interacting water masses (Figures 2b–2i; Table S1 in Supporting Information S1).

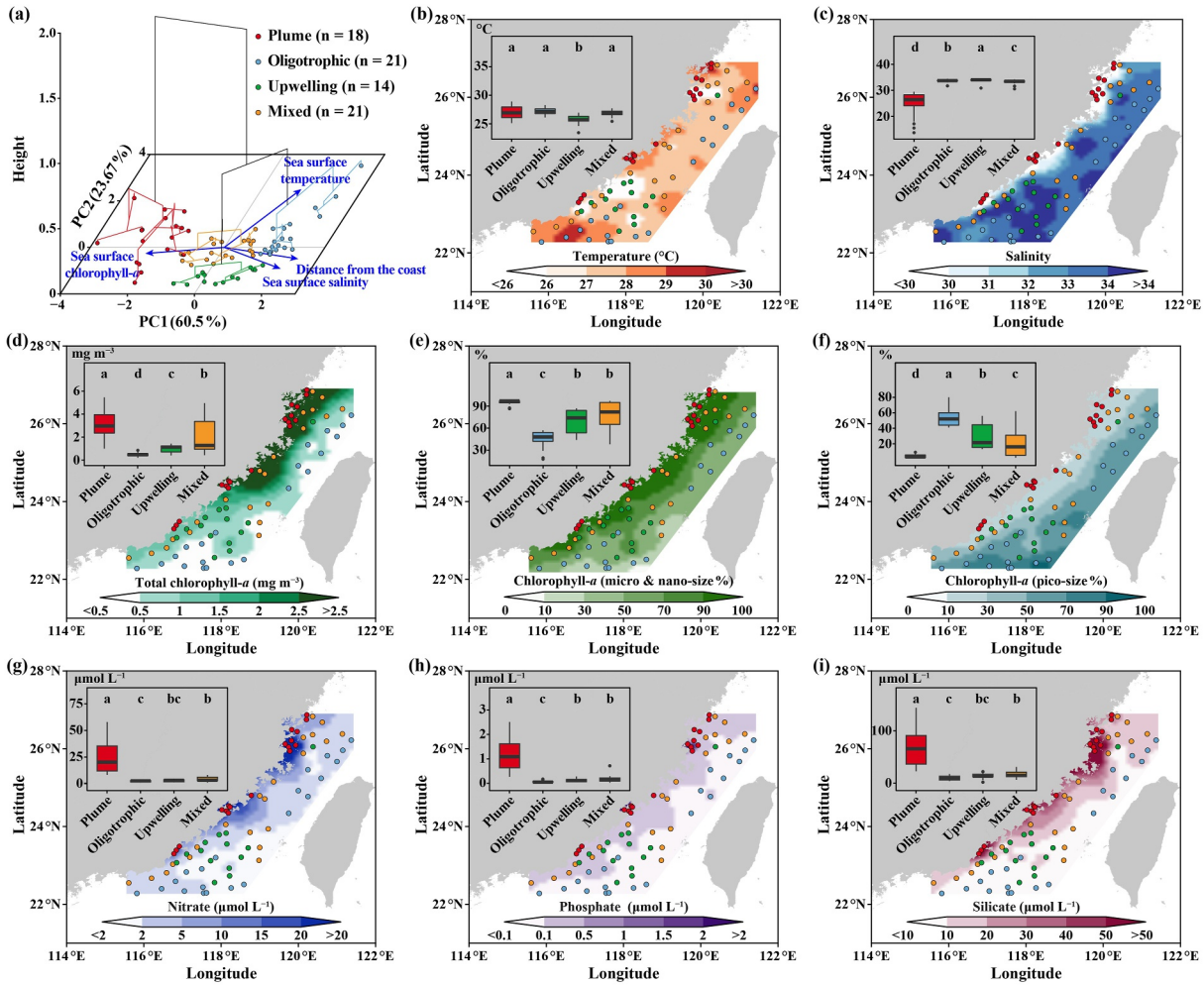


**Figure 2.** Environmental characteristics of different ecological regimes in the Taiwan Strait. (a) Identification of ecological regimes via cluster analysis. The principal component analysis displays individual sampling stations (dots) and loadings of key environmental variables (arrows), and the dendrogram illustrates the dissimilarity between stations, which were classified into four ecological regimes based on similar hydrographic and biological characteristics. Panels (b–i) show spatial distributions of (b) temperature, (c) salinity, (d) chlorophyll-*a* concentrations, (e) the combined fraction of micro- and nanophytoplankton to total chlorophyll-*a*, (f) picophytoplankton fraction to total chlorophyll-*a*, (g) nitrate, (h) phosphate, and (i) silicate, respectively. Stations on the maps are colored according to the four ecological regimes identified by cluster analysis in panel (a). Box plots show the variation of each variable across the four ecological regimes, with distinct letters above the boxes denoting statistically significant differences among the regimes ($p < 0.05$). All variables were integrated over the euphotic zone and normalized by euphotic depth.

### 3.2. Bacterial Metabolism Across Environmental Gradients

Bacterial carbon metabolism exhibited pronounced spatial heterogeneity across the study region. Overall, euphotic-zone averaged BCD decreased markedly from nearshore to offshore waters, spanning a wide range from 760.56 to 24.96 mg C $m^{-3}$ $d^{-1}$, whereas BGE displayed an opposite offshore-increasing trend, ranging from 43% to 1% (Figures 3a and 3b). Among the four ecological regimes, the plume and mixed water regions exhibited the highest BCD, with mean values of 309.6 ± 227.0 and 228.0 ± 184.0 mg C $m^{-3}$ $d^{-1}$, respectively. Intermediate BCD values were observed in the upwelling region (119.6 ± 70.1 mg C $m^{-3}$ $d^{-1}$), while the oligotrophic region showed substantially lower BCD, averaging only 50.6 ± 29.5 mg C $m^{-3}$ $d^{-1}$ (Figure 3c). Across all stations, BR constituted the dominant component of BCD (Figure 3a). Absolute BR rates were highest in the plume and mixed water regions, reaching 295.15 ± 225.07 and 206.26 ± 180.93 mg C $m^{-3}$ $d^{-1}$, respectively. The upwelling region exhibited moderate BR rates (97.97 ± 65.72 mg C $m^{-3}$ $d^{-1}$), whereas the oligotrophic region showed the lowest BR values (38.42 ± 26.08 mg C $m^{-3}$ $d^{-1}$) (Figure 3d). In contrast, BP peaked in the upwelling and mixed water regions (21.58 ± 7.48 and 21.75 ± 8.07 mg C $m^{-3}$ $d^{-1}$, respectively) and remained lower in plume (14.49 ± 5.72 mg C $m^{-3}$ $d^{-1}$) and oligotrophic waters (12.17 ± 4.41 mg C $m^{-3}$ $d^{-1}$) (Figure 3e). Consequently,

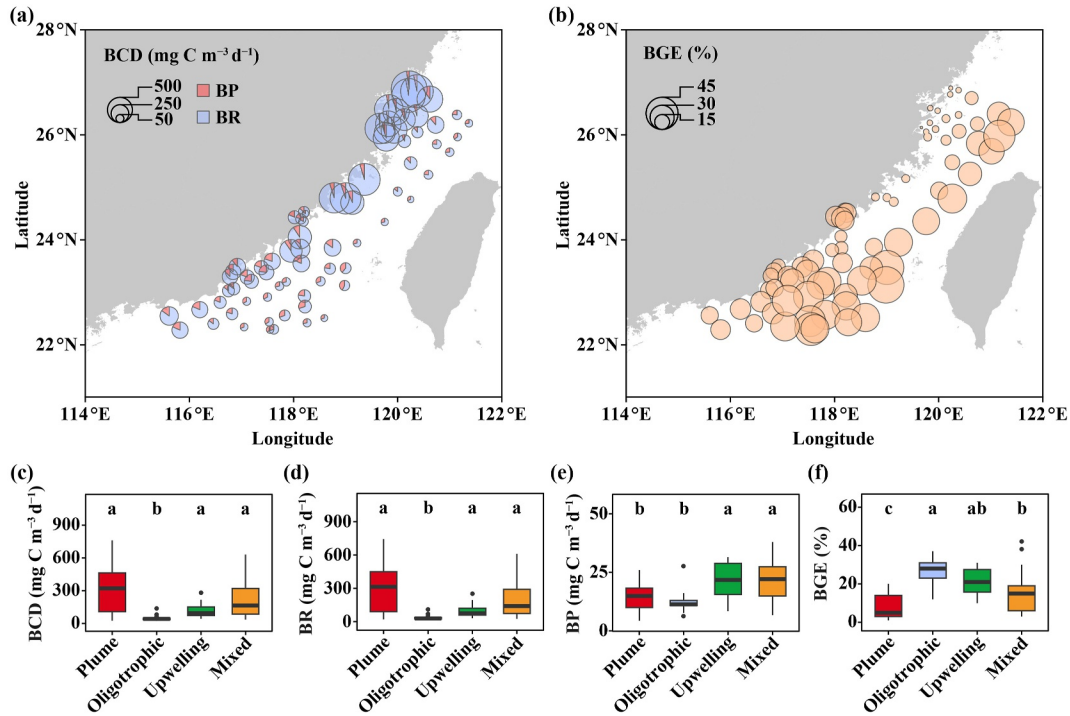


**Figure 3.** Bacterial carbon metabolism across ecological regimes in the Taiwan Strait. (a) Spatial distribution of bacterial carbon demand (BCD) across sampling stations. Pie size indicates the magnitude of BCD, while colors represent the relative contributions of bacterial production (BP) and bacterial respiration (BR) to total BCD. (b) Spatial distribution of bacterial growth efficiency (BGE) across stations. (c–f) Box plots show the variation of (c) BCD, (d) BR, (e) BP, and (f) BGE across the four ecological regimes, with distinct letters above the boxes denoting statistically significant differences among regimes ($p < 0.05$). All variables were integrated over the euphotic zone and normalized by euphotic depth.

the oligotrophic region exhibited the highest contribution of BP to BCD (BGE = 27% ± 7%), followed by the upwelling region (BGE = 21% ± 8%), whereas plume and mixed water regions, despite their elevated BCD, showed comparatively low BGE (9% ± 7% and 15% ± 11%, respectively) (Figure 3f).

### 3.3. Phytoplankton-Derived Particulate and Dissolved Organic Carbon Production Across Environmental Gradients

Spatial patterns of phytoplankton primary production mirrored those of bacterial carbon metabolism across the study region (Figures 4a and 4b). Euphotic-zone averaged TPP ranged from 26.40 to 638.40 mg C $m^{-3}$ $d^{-1}$, highest in the plume region (395.4 ± 160.6 mg C $m^{-3}$ $d^{-1}$), followed by the mixed water (224.8 ± 126.3 mg C $m^{-3}$ $d^{-1}$) and upwelling regions (176.3 ± 111.7 mg C $m^{-3}$ $d^{-1}$), and lowest in the oligotrophic region (54.1 ± 23.2 mg C $m^{-3}$ $d^{-1}$) (Figure 4c). Across all ecological regimes, TPP was dominated by PPP (Figure 4a). This dominance was most pronounced in the plume, upwelling, and mixed water regions, where PPP averaged 371.19 ± 148.42, 193.33 ± 116.05, and 153.05 ± 104.98 mg C $m^{-3}$ $d^{-1}$, respectively (Figure 4d). In contrast, DPP varied less among these productive regimes (ranged from 24.21 to 31.39 mg C $m^{-3}$ $d^{-1}$) and accounted for only a small fraction of TPP (PER = 13% ± 8%) (Figures 4e and 4f). In the oligotrophic region, both PPP and DPP were substantially reduced (38.99 ± 17.21 and 15.13 ± 7.16 mg C $m^{-3}$ $d^{-1}$, respectively), yet the relative contribution of DPP to TPP increased markedly compared to the other three regimes (PER = 28% ± 7%) (Figure 4d–4f). This shift indicates a fundamental change in carbon partitioning along the trophic gradient, with oligotrophic waters channeling a larger fraction of primary production directly into the dissolved pool.

### 3.4. Drivers of Bacterial Metabolism and Primary Production

Correlation analyses revealed clear linkages between bacterial carbon metabolism, phytoplankton primary production, and environmental conditions across the study region. BCD was strongly and positively correlated with

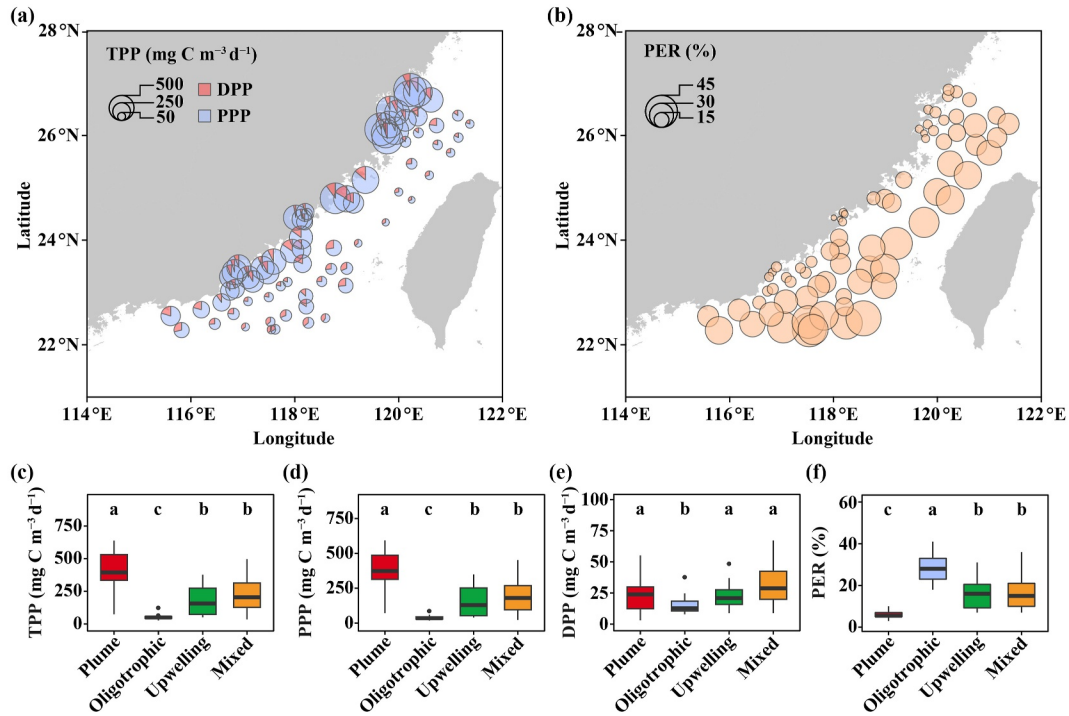


**Figure 4.** Phytoplankton primary production across ecological regimes in the Taiwan Strait. (a) Spatial distribution of total primary production (TPP) across sampling stations. Pie size indicates the magnitude of TPP, while colors represent the relative contributions of dissolved primary production (DPP) and particulate primary production (PPP) to TPP. (b) Spatial distribution of the proportion of DPP relative to TPP (PER). (c–f) Box plots illustrate the variation of (c) TPP, (d) PPP, (e) DPP, and (f) PER across the four ecological regimes, with distinct letters above the boxes denoting statistically significant differences among regimes ($p < 0.05$). All variables were integrated over the euphotic zone and normalized by euphotic depth.

TPP ($r = 0.90$, $p < 0.001$; Figure 5a), indicating that phytoplankton production provides the dominant organic carbon source sustaining bacterial metabolism. This relationship was closely associated with higher concentrations of nitrate, phosphate, and silicate, lower N:P ratios, elevated chlorophyll-*a*, and greater contributions of micro- and nanophytoplankton (Figure 5a). Different processes of bacterial metabolism exhibited distinct correlations with phytoplankton-derived carbon pools: BR was more strongly correlated with PPP ($r = 0.89$, $p < 0.001$) than with DPP ($r = 0.78$, $p < 0.001$), while BP showed a stronger association with DPP ($r = 0.75$, $p < 0.001$) than with PPP ($r = 0.46$, $p < 0.001$) (Figures 5b and 5c). Accordingly, BGE increased significantly with PER ($r = 0.62$, $p < 0.001$), a pattern most evident under low-nutrient, low-chlorophyll, and low-productivity conditions dominated by picophytoplankton (Figure 5d). In addition, the ratio of BCD to TPP was positively correlated with PER ($r = 0.37$, $p < 0.001$; Figure 5a).

Partial least squares path modeling further reveals a trophic cascade in which nutrient availability is linked to changes in phytoplankton size structure, which in turn affects the partitioning of primary production and subsequent bacterial metabolic responses (Figure 5e). Specifically, high-nutrient environments and phytoplankton communities dominated by micro- and nanophytoplankton were accompanied by a larger fraction of PPP and respiration-dominated bacterial metabolism, whereas low-nutrient conditions and picophytoplankton-dominated communities corresponded to higher PER and correspondingly higher BGE.

## 4. Discussion

### 4.1. Phytoplankton-Derived Carbon Partitioning and Its Association With Bacterial Growth Efficiency

Across the Taiwan Strait, DPP constituted a nontrivial fraction of TPP, with a regional mean contribution of 17% (Figure 4). In absolute terms, DPP increased with PPP, indicating that highly productive, nutrient-replete waters dominated by larger phytoplankton exhibited elevated DOC release (Figure 5a). When expressed as a fraction of

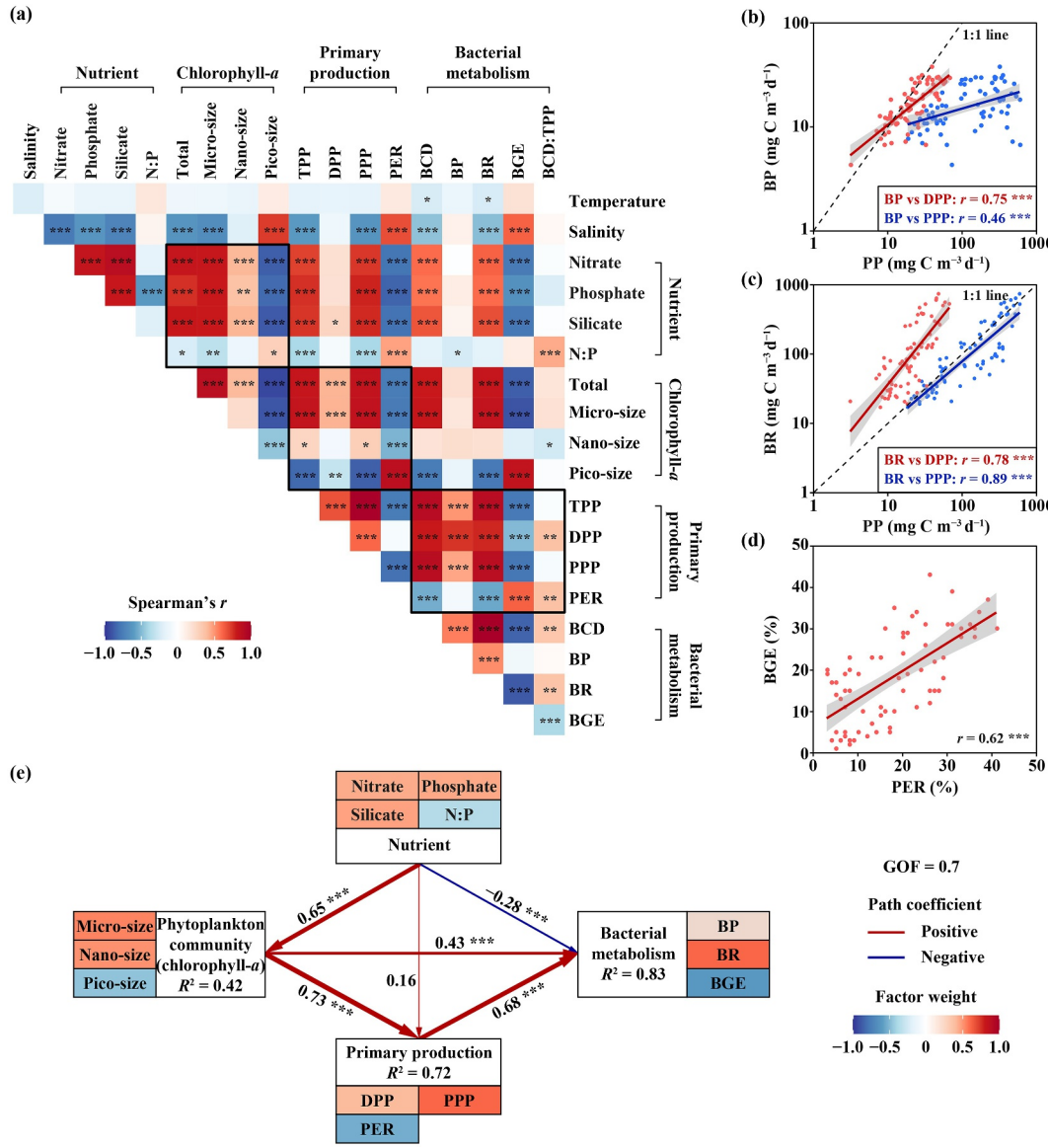


**Figure 5.** Correlation analysis of bacterial carbon metabolism, primary production, and environmental variables across stations. (a) Correlation matrix among multiple variables. Heatmap colors indicate Spearman rank correlation coefficients, with black outlines highlighting variable combinations showing the strongest ecological associations. TPP: total primary production; DPP: dissolved primary production; PPP: particulate primary production; PER: percent extracellular release; BCD: bacterial carbon demand; BP: bacterial production; BR: bacterial respiration; BGE: bacterial growth efficiency. (b) Relationships of BP with dissolved primary production (DPP) and particulate primary production (PPP). (c) Relationships of BR with DPP and PPP. (d) Relationship between bacterial growth efficiency and percent extracellular release. (e) Partial least squares path modeling depicting direct and indirect relationships multiple variables. Node color intensity corresponds to the relative importance (weights) of individual variables within each latent construct as determined by model loadings, while arrows represent standardized path coefficients. Significance levels are indicated as $*p < 0.05$, $**p < 0.01$, and $***p < 0.001$ in all panels. All variables were integrated over the euphotic zone and normalized by euphotic depth.

total production, however, the relative contribution of dissolved production (PER) exhibited a contrasting pattern. PER showed a clear inverse relationship with productivity and differed markedly among water masses. High-nutrient, high-productivity plume, upwelling, and mixed water regions consistently displayed low PER values (generally <20%), whereas the oligotrophic offshore region dominated by picophytoplankton showed the highest PER (with a maximum of 41%) (Figure 4f). This spatial pattern closely aligns with observations from other

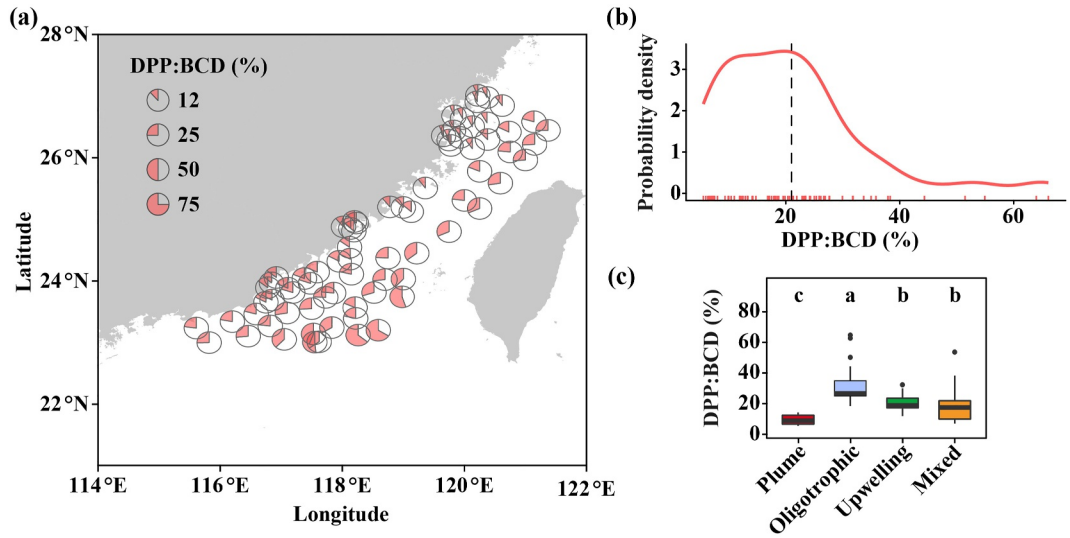


**Figure 6.** Contribution of phytoplankton dissolved primary production (DPP) to bacterial carbon demand (BCD). (a) Spatial distribution of the fractional contribution of DPP to BCD across sampling stations. Size of all the Pie chart in the panel a is identical, with the red sector representing the fractional proportion contributed by DPP. (b) Probability density distribution of the DPP-to-BCD ratio, with the dashed line indicating the mean value. (c) The box plot shows the DPP-to-BCD ratio across the four ecological regimes, with distinct letters above the boxes denoting statistically significant differences among regimes ($p < 0.05$). All variables were integrated over the euphotic zone and normalized by euphotic depth.

tropical and subtropical systems, where PER typically remains below 20% in eutrophic coastal and upwelling environments but increases to 30%–60% under oligotrophic conditions (Boulion, 2021; Kang et al., 2024; Mühlenbruch et al., 2018; Poulton et al., 2016; Thornton, 2014). The underlying mechanism driving the PER is commonly attributed to nutrient limitation of phytoplankton growth. Under sufficient light availability, phytoplankton can continue to fix $CO_2$; however, shortages of nitrogen or phosphorus constrain the incorporation of fixed carbon into biomass. Excess photosynthetically fixed carbon can therefore be redirected into multiple pathways, including the production of storage compounds (e.g., labile polysaccharides), increased respiratory losses, and extracellular release of DOC (Halsey & Jones, 2015). Among these pathways, DOC release has been widely observed as a response that helps maintain cellular metabolic balance and alleviates photophysiological stress (Carlson & Hansell, 2015; Moran, Ferrer-González, et al., 2022; Thornton, 2014).

At the regional scale, BCD was tightly coupled to TPP, indicating that phytoplankton primary production constitutes the dominant ultimate carbon source supporting bacterial heterotrophic metabolism in the Taiwan Strait (Figures 3a and 4a, and 5a). Results from partial least squares path modeling further suggested a coherent linkage among nutrient availability, phytoplankton size structure, primary production partitioning, and bacterial metabolic responses (Figure 5e). Higher nutrient availability was associated with shifts in phytoplankton communities toward larger size classes, along with increased TPP and reduced relative DOC release, which were in turn associated with more respiration-dominated bacterial metabolism (Prakash et al., 2024; Robinson, 2008).

Notably, despite its importance, DPP fluxes were insufficient to independently satisfy total BCD at nearly all stations (Figures 6a and 6b). Spatially, the study domain was characterized by uniformly low DPP:BCD ratios, where DPP accounted for merely 21% of BCD on average. Distinct differences among water masses further highlight this imbalance (Figure 6c). The plume region showed the lowest DPP:BCD ratios, while upwelling and mixed waters exhibited moderately higher values but still remained well below 30%. Even in oligotrophic waters with the highest fractions of extracellularly released primary production, DPP fluxes at most stations still failed to reach half of BCD. Similar imbalances between DPP supply and BCD have been widely reported, with phytoplankton-released DOC commonly accounting for only 10%–30% of BCD (Carreira et al., 2021; Chen et al., 2020; Fouilland & Mostajir, 2010; Kang et al., 2022; Lu et al., 2025). These results indicate that bacterial metabolism at the regional scale remains largely dependent on secondary DOC regenerated from POC through food web processing.

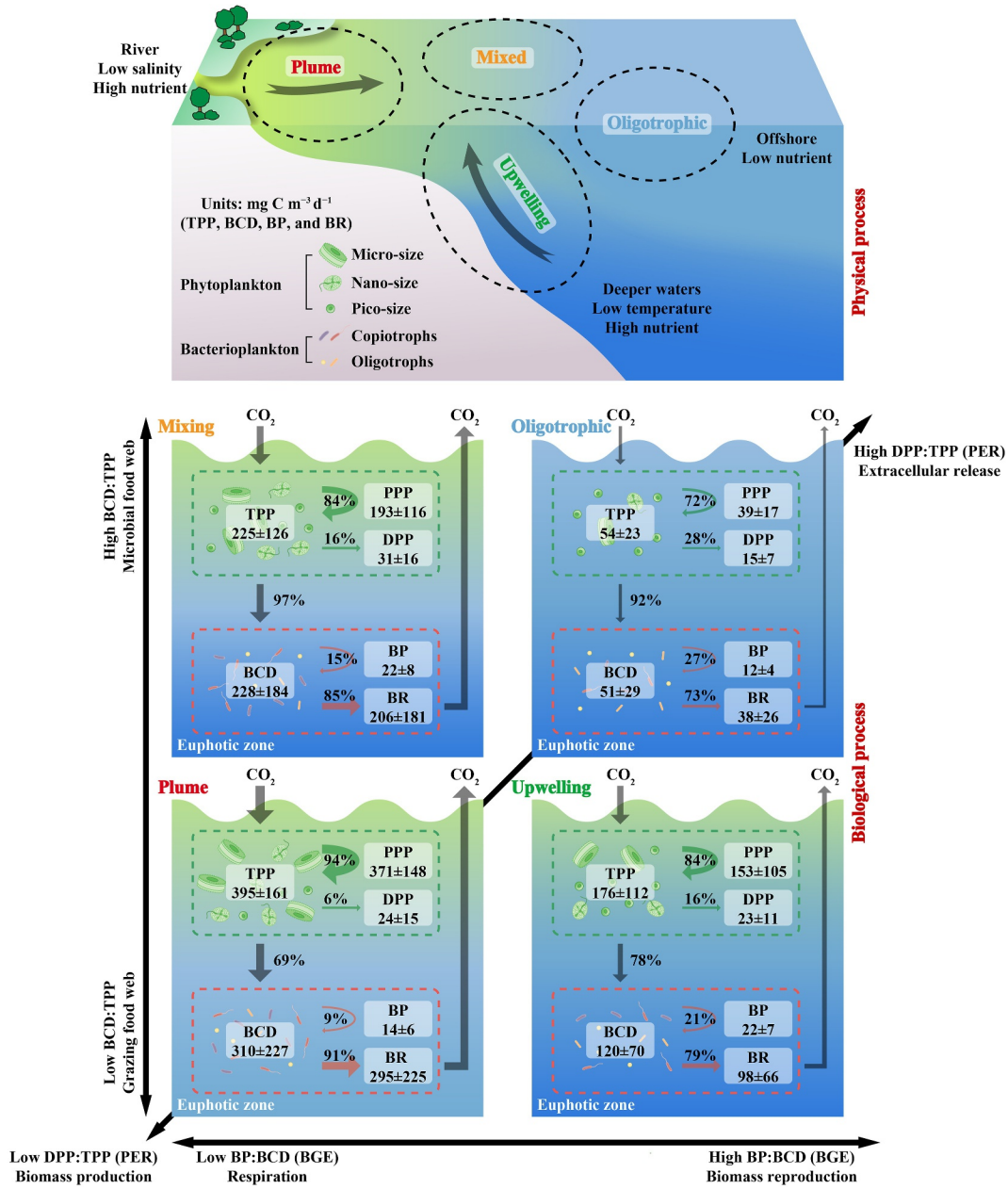


**Figure 7.** Conceptual diagram illustrating contrasting bacteria-phytoplankton carbon flow structures across different water masses in the Taiwan Strait. TPP: total primary production; DPP: dissolved primary production; PPP: particulate primary production; PER: percent extracellular release; BCD: bacterial carbon demand; BP: bacterial production; BR: bacterial respiration; BGE: bacterial growth efficiency.

Interestingly, although DPP alone cannot meet BCD, its relative contribution to primary production is closely linked to variations in BGE. We observed that BR correlated more strongly with PPP, whereas BP showed a tighter association with DPP (Figures 5b and 5c). As a consequence, increases in PER were consistently accompanied by higher BGE across the study region (Figures 3f, 4f, and 5d), suggesting a coordinated response between phytoplankton carbon allocation strategies and bacterial carbon use efficiency. One possible explanation for these associations lies in differences in the biochemical composition and lability of organic matter derived from distinct primary production pathways. DPP is typically composed of low-molecular-weight, chemically labile compounds that can be readily assimilated by bacteria (Moran et al., 2022a, 2022b). In oligotrophic waters with elevated PER, microbial communities are often dominated by free-living bacteria, which generally possess

high substrate affinities and efficient uptake capabilities, potentially favoring biomass production and contributing to higher BGE (Arandia-Gorostidi et al., 2017; Middelboe et al., 1995). In contrast, organic carbon derived from PPP and subsequently processed through the food web is often more structurally complex (Arnosti, 2011; Kujawinski, 2011), and its utilization may involve higher metabolic costs. In environments where PER is low and bacterial metabolism relies more heavily on PPP-derived carbon, particle-associated bacteria are often more prevalent. These bacteria exhibit enhanced extracellular enzyme production and metabolic versatility, enabling the breakdown of complex polymers into utilizable substrates (Arandia-Gorostidi et al., 2017; Azam & Long, 2001; Baumas et al., 2021). However, extracellular enzyme synthesis and particle-associated metabolism can be energetically demanding, potentially leading to higher respiratory losses and lower BGE.

While the mechanisms outlined above provide a plausible explanation for the observed co-variation between PER and BGE, they are mostly based on correlational inference rather than direct causal evidence, and the role of DOC composition is implied but not explicitly measured. Importantly, particulate organic matter can also generate highly labile substrates through enzymatic hydrolysis and particle-associated microbial activity, leading to localized "hotspots" of elevated bacterial activity (Baumas et al., 2023; Moran, Kujawinski, et al., 2022). Thus, dissolved and particulate production pathways likely differ not simply in lability but also in the form, timing, and accessibility of organic substrates supplied to bacterial communities. In addition, the observed co-variation between PER and BGE may also reflect the influence of other environmental gradients. Future work incorporating direct characterization of DOC quality and microbial community composition will be required to disentangle these mechanisms and establish causality.

### 4.2. Contrasting Carbon Flow Pathways Across Water Masses

Building on the linkage between primary production partitioning and BGE identified above, we next analyzed how this coupling translates into contrasting carbon flow structures across distinct water masses. The pronounced water mass heterogeneity of the Taiwan Strait provides an ideal framework for examining how physical settings regulate bacteria-phytoplankton coupling and associated carbon flow structures. Based on cluster analysis, four representative water masses were identified: plume waters, oligotrophic waters, upwelling waters, and mixed waters (Figure 2a). To systematically compare carbon flow pathways among these regimes, we established an integrated framework comprising three complementary metrics (Figure 7): (a) PER, reflecting phytoplankton carbon allocation strategy; (b) the ratio of BCD to TPP (BCD:TPP), indicating the strength of microbial relative to newly produced organic carbon by phytoplankton; and (c) BGE, describing the efficiency of bacterial carbon assimilation.

Marked differences in biological metrics reveal fundamentally different modes of carbon processing among water masses. The oligotrophic regime represents one endmember characterized by a "high PER–high BCD:TPP–high BGE" pattern (Figure 7). Here, a large fraction of newly fixed carbon is processed through bacterial metabolism, consistent with the strong role of the microbial loop. Elevated BGE (~27%) suggests relatively efficient bacterial carbon retention under nutrient-limited conditions, potentially driven by enhanced DOC release from picophytoplankton and rapid assimilation of labile substrates by free-living, high-affinity bacteria (Mühlenbruch et al., 2018; Poulton et al., 2016; Thornton, 2014). At the opposite endmember, plume waters exhibit a "low PER–low BCD:TPP–low BGE" structure associated with intense particulate production by micro- and nanophytoplankton (PPP ≈ 94% of TPP) (Figure 7). Lower BCD:TPP suggests that a greater fraction of organic carbon is transferred through the classical food chain, thereby reducing direct microbial access. The markedly low BGE (~9%) reflects respiration-dominated bacterial metabolism, potentially linked to the energetic costs of processing particle-associated organic matter and the influence of more refractory, terrestrially derived carbon inputs (Bianchi, 2011; Mühlenbruch et al., 2018; Zhao et al., 2019).

Upwelling and mixed waters occupy intermediate productivity levels but diverge sharply in carbon flow organization despite exhibiting similar PER values (~16%–17%; Figure 4f), indicating that phytoplankton carbon partitioning alone does not determine bacterial metabolic responses. Upwelling waters display a "mid PER–low BCD:TPP–high BGE" structure, reflecting a relatively stable balance between particulate and dissolved production (Figure 7). Sustained nutrient supply supports continuous phytoplankton growth, providing both trophic transfer via PPP and a steady input of bioavailable DOC that fuels efficient bacterial biomass synthesis (Cai et al., 2024; Moran, Ferrer-González, et al., 2022; Pontiller et al., 2022). In contrast, mixed waters exhibit a "mid PER–high BCD:TPP–low BGE" configuration, with BCD:TPP approaching or exceeding unity, indicative of

near-balanced or weakly net heterotrophic conditions (Figure 7). This pattern may arise from strong temporal variability associated with water mass mixing. Episodic nutrient inputs can generate short pulses of fresh organic matter, but phytoplankton production may not be sustained (Mahadevan, 2016). As a result, labile DOC may be rapidly depleted while bacterial metabolic demand remains elevated, potentially increasing reliance on more refractory carbon pools and leading to higher respiratory costs and lower growth efficiency. This temporal decoupling between carbon supply and microbial demand gives rise to a carbon flow structure distinct from both stable upwelling systems and productivity-dominated plume waters.

### 4.3. Implications for Carbon Cycles

Taken together, our results highlight that DPP represents a quantitatively and functionally important component of primary production, and is closely linked to bacterial carbon utilization strategies. DPP introduces an additional pathway in marine carbon cycling by routing fixed carbon through the dissolved phase, directly linking phytoplankton production to the microbial loop (Moran et al., 2022a, 2022b). Although DPP alone is insufficient to satisfy total bacterial metabolic demand (Figure 6), variation in its relative contribution to primary production is consistently associated with changes in BGE (Figure 5d). In particular, climate-driven increases in upper-ocean stratification and reduced nutrient supply are expected to drive primary production toward a greater proportion of extracellular release as DPP (Flanjak et al., 2025), which may in turn be linked to shifts in bacterial metabolic balance and carbon retention within the upper ocean.

Furthermore, the ratio of carbon transfer from phytoplankton to bacteria (BCD:TPP) appears to have little dependence on TPP, but is instead linked to DPP generation (Figures 5a and 7). This suggests that microbial processing pathways largely govern the fate of carbon originating from DPP, with important consequences for ocean carbon sequestration. Under low BGE, a substantial fraction of DOC is respired in surface waters, limiting its contribution to carbon export (Del Giorgio & Cole, 1998). In contrast, higher BGE may promote the conversion of DOC into bacterial biomass, enhancing its potential transfer to particulate pathways or higher trophic levels, or sequestration as refractory DOC via the microbial carbon pump (Del Giorgio & Cole, 1998; Jiao et al., 2010). In addition, a fraction of DOC may escape rapid microbial utilization and be transported to depth via physical processes such as mixing or subduction, contributing to longer-term carbon storage (Roshan & DeVries, 2017). Although our data do not allow a quantitative estimate of the contribution of DPP-derived DOC to carbon export and long-term storage, they provide important observational constraints on the pathways through which this carbon may be processed. A more comprehensive assessment will require improved constraints on DOC production, transformation, and transport, including its chemical composition, microbial utilization, and physical export pathways.

## 5. Conclusions

Based on multi-cruise observations in the highly dynamic subtropical Taiwan Strait, this study simultaneously quantified bacterial metabolism and phytoplankton primary production partitioned into dissolved and particulate carbon pools. Our results show that bacterial carbon metabolism is closely associated with a cascade linking nutrient supply, phytoplankton size structure, and the partitioning of primary production between dissolved and particulate carbon pools. Although DPP alone cannot satisfy total bacterial metabolic demand, its relative contribution to primary production is strongly associated with variations in BGE. Higher DPP fractions are linked to more efficient bacterial biomass synthesis, whereas systems dominated by particulate production are associated with enhanced respiratory carbon loss. In addition, physical dynamics—including riverine inputs, upwelling, and water mass mixing—are associated with variations in microbial carbon flow pathways and corresponding differences in carbon utilization strategies across water masses.

Our results provide an observational baseline for understanding how microbial carbon flow structures may respond to environmental change in subtropical marginal seas, which are strongly influenced by land-ocean-atmosphere interactions. However, this study focuses on the southwest monsoon period, when physical forcing is strongest. Extending similar observations to the northeast monsoon season will be essential to resolve the full seasonal variability of bacteria-phytoplankton coupling and carbon flow dynamics. Together, these findings improve our understanding of how biological and physical processes jointly influence microbial carbon cycling in dynamic coastal systems under a changing climate.

## Conflict of Interest

The authors declare no conflicts of interest relevant to this study.

## Availability Statement

Field cruise data used in this study are available in Liu et al. (2026). NASA Ocean Color products for monthly sea surface temperature and chlorophyll-*a* concentrations can be accessed at https://oceancolor.gsfc.nasa.gov/l3/. Monthly sea surface salinity data can be accessed from Global Ocean Physics Reanalysis. Copernicus. [Data set] https://doi.org/10.48670/moi-00021.

**Acknowledgments**
This work was supported by the National Natural Science Foundation of China (Grant 42406099), the Scientific Research Foundation of Third Institute of Oceanography, Ministry of Natural Resources (Grant 2024009), the Natural Science Foundation of Fujian Province, China (2024J01182 and 2025J09005), Natural Science Foundation of Xiamen, China (Grant 3502Z202472006), and Fundamental Research Funds for the Central Universities (Grant 20720240105 and 20720240053).

## References

Arandia-Gorostidi, N., Weber, P. K., Alonso-Sáez, L., Morán, X. A. G., & Mayali, X. (2017). Elevated temperature increases carbon and nitrogen fluxes between phytoplankton and heterotrophic bacteria through physical attachment. *ISME Journal*, *11*(3), 641–650. https://doi.org/10.1038/ismej.2016.156

Arnosti, C. (2011). Microbial extracellular enzymes and the marine carbon cycle. *Annual Review of Marine Science*, *3*(1), 401–425. https://doi.org/10.1146/annurev-marine-120709-142731

Azam, F. (1998). Microbial control of oceanic carbon flux: The plot thickens. *Science*, *280*(5364), 694–696. https://doi.org/10.1126/science.280.5364.694

Azam, F., & Long, R. A. (2001). Sea snow microcosms. *Nature*, *414*(6863), 495–498. https://doi.org/10.1038/35107174

Azam, F., & Malfatti, F. (2007). Microbial structuring of marine ecosystems. *Nature Reviews Microbiology*, *5*(10), 782–791. https://doi.org/10.1038/nrmicro1747

Baumas, C. M. J., Fuchs, R., Garel, M., Poggiale, J.-C., Memery, L., Le Moigne, F. A. C., & Tamburini, C. (2023). Reconstructing the ocean's mesopelagic zone carbon budget: Sensitivity and estimation of parameters associated with prokaryotic remineralization. *Biogeosciences*, *20*(19), 4165–4182. https://doi.org/10.5194/bg-20-4165-2023

Baumas, C. M. J., Le Moigne, F. A. C., Garel, M., Bhairy, N., Guasco, S., Riou, V., et al. (2021). Mesopelagic microbial carbon production correlates with diversity across different marine particle fractions. *ISME Journal*, *15*(6), 1695–1708. https://doi.org/10.1038/s41396-020-00880-z

Bianchi, T. S. (2011). The role of terrestrially derived organic carbon in the coastal ocean: A changing paradigm and the priming effect. *Proceedings of the National Academy of Sciences*, *108*(49), 19473–19481. https://doi.org/10.1073/pnas.1017982108

Boulion, V. (2021). Extracellular phytoplankton production and its importance for heterotrophic activity of bacteria. *Biology Bulletin*, *48*(3), 358–366. https://doi.org/10.1134/S1062359021030043

Cai, L., Li, H., Deng, J., Zhou, R., & Zeng, Q. (2024). Biological interactions with *Prochlorococcus*: Implications for the marine carbon cycle. *Trends in Microbiology*, *32*(3), 280–291. https://doi.org/10.1016/j.tim.2023.08.011

Carlson, C. A., & Hansell, D. A. (2015). DOM sources, sinks, reactivity, and budgets. *Biogeochemistry of marine dissolved organic matter*, 65–126. https://doi.org/10.1016/B978-0-12-405940-5.00003-0

Carreira, C., Talbot, S., & Lønborg, C. (2021). Bacterial consumption of total and dissolved organic carbon in the Great Barrier Reef. *Biogeochemistry*, *154*(3), 489–508. https://doi.org/10.1007/s10533-021-00802-x

Chen, B., Huang, B., Xie, Y., Guo, C., Song, S., Li, H., & Liu, H. (2014). The bacterial abundance and production in the East China Sea: Seasonal variations and relationships with the phytoplankton biomass and production. *Acta Oceanologica Sinica*, *33*(9), 166–177. https://doi.org/10.1007/s13131-014-0528-0

Chen, C.-C., Chou, W.-C., Hung, C.-C., & Gong, G.-C. (2024). Nutrient sources, phytoplankton blooms, and hypoxia along the Chinese coast in the East China Sea: Insight from summer 2014. *Marine Pollution Bulletin*, *205*, 116692. https://doi.org/10.1016/j.marpolbul.2024.116692

Chen, T.-Y., Lai, C.-C., Shiah, F.-K., & Gong, G.-C. (2020). Dissolved and particulate primary production and subsequent bacterial C consumption in the Southern East China Sea. *Frontiers in Marine Science*, *7*, 713. https://doi.org/10.3389/fmars.2020.00713

Chen, Z., Yan, X. H., & Jiang, Y. (2014). Coastal cape and canyon effects on wind-driven upwelling in northern Taiwan Strait. *Journal of Geophysical Research: Oceans*, *119*(7), 4605–4625. https://doi.org/10.1002/2014jc009831

Cloern, J. E., Foster, S. Q., & Kleckner, A. E. (2014). Phytoplankton primary production in the world's estuarine-coastal ecosystems. *Biogeosciences*, *11*(9), 2477–2501. https://doi.org/10.5194/bg-11-2477-2014

Crump, B. C., & Bowen, J. L. (2024). The microbial ecology of estuarine ecosystems. *Annual Review of Marine Science*, *16*(1), 335–360. https://doi.org/10.1146/annurev-marine-022123-101845

Dai, M., Su, J., Zhao, Y., Hofmann, E. E., Cao, Z., Cai, W.-J., et al. (2022). Carbon fluxes in the coastal ocean: Synthesis, boundary processes, and future trends. *Annual Review of Earth and Planetary Sciences*, *50*(1), 593–626. https://doi.org/10.1146/annurev-earth-032320-090746

Del Giorgio, P. A., & Cole, J. J. (1998). Bacterial growth efficiency in natural aquatic systems. *Annual Review of Ecology and Systematics*, *29*(1), 503–541. https://doi.org/10.1146/annurev.ecolsys.29.1.503

Del Giorgio, P. A., Cole, J. J., & Cimbleris, A. (1997). Respiration rates in bacteria exceed phytoplankton production in unproductive aquatic systems. *Nature*, *385*(6612), 148–151. https://doi.org/10.1038/385148a0

Del Giorgio, P. A., Condon, R., Bouvier, T., Longnecker, K., Bouvier, C., Sherr, E., & Gasol, J. M. (2011). Coherent patterns in bacterial growth, growth efficiency, and leucine metabolism along a northeastern Pacific inshore-offshore transect. *Limnology and Oceanography*, *56*(1), 1–16. https://doi.org/10.4319/lo.2011.56.1.0001

DeVries, T. (2022). The ocean carbon cycle. *Annual Review of Environment and Resources*, *47*(1), 317–341. https://doi.org/10.1146/annurev-environ-120920-111307

Ducklow, H. (2000). Bacterial production and biomass in the oceans. In *Microbial ecology of the oceans* (pp. 85–120). Wiley

Flanjak, L., Wienkers, A., & Laufkötter, C. (2025). Dissolved organic carbon dynamics in a changing ocean: An ESM2M-COBALTv2 coupled model analysis. *Biogeosciences*, *22*(22), 6877–6894. https://doi.org/10.5194/bg-22-6877-2025

Fouilland, E., & Mostajir, B. (2010). Revisited phytoplanktonic carbon dependency of heterotrophic bacteria in freshwaters, transitional, coastal and oceanic waters. *FEMS Microbiology Ecology*, *73*(3), 419–429. https://doi.org/10.1111/j.1574-6941.2010.00896.x

Grasshoff, K., Kremling, K., & Ehrhardt, M. (1999). *Methods of seawater analysis*. Wiley. https://doi.org/10.1002/9783527613984

Guo, C., Ke, Y., Chen, B., Zhang, S., & Liu, H. (2022). Making comparable measurements of bacterial respiration and production in the subtropical coastal waters. *Marine Life Science & Technology*, *4*(3), 414–427. https://doi.org/10.1007/s42995-022-00133-2

Halsey, K. H., & Jones, B. M. (2015). Phytoplankton strategies for photosynthetic energy allocation. *Annual Review of Marine Science*, *7*(1), 265–297. https://doi.org/10.1146/annurev-marine-010814-015813

Hama, T., Miyazaki, T., Ogawa, Y., Iwakuma, T., Takahashi, M., Otsuki, A., & Ichimura, S. (1983). Measurement of photosynthetic production of a marine phytoplankton population using a stable $^{13}C$ isotope. *Marine Biology*, *73*(1), 31–36. https://doi.org/10.1007/bf00396282

Hansell, D. A., & Orellana, M. V. (2021). Dissolved organic matter in the global ocean: A primer. *Gels*, *7*(3), 128. https://doi.org/10.3390/gels7030128

Heneghan, R. F., Holloway-Brown, J., Gasol, J. M., Herndl, G. J., Moran, X. A. G., & Galbraith, E. D. (2024). The global distribution and climate resilience of marine heterotrophic prokaryotes. *Nature Communications*, *15*(1), 6943. https://doi.org/10.1038/s41467-024-50635-z

Huang, Y., Fassbender, A. J., Long, J. S., Johannessen, S., & Bernardi Bif, M. (2022). Partitioning the export of distinct biogenic carbon pools in the northeast Pacific Ocean using a biogeochemical profiling float. *Global Biogeochemical Cycles*, *36*(2), e2021GB007178. https://doi.org/10.1029/2021gb007178

Jiao, N., Herndl, G. J., Hansell, D. A., Benner, R., Kattner, G., Wilhelm, S. W., et al. (2010). Microbial production of recalcitrant dissolved organic matter: Long-term carbon storage in the global ocean. *Nature Reviews Microbiology*, *8*(8), 593–599. https://doi.org/10.1038/nrmicro2386

Kang, J., Liu, X., Lin, X., Chen, X., Luo, Z., & Huang, B. (2024). Biogeochemical factors regulating photosynthetically dissolved organic carbon produced by phytoplankton in the Taiwan Strait. *Environmental Research*, *252*(4), 119090. https://doi.org/10.1016/j.envres.2024.119090

Kang, J., Luo, Z., Mohamed, H. F., Lin, Y., Huang, S., Wang, Y., & Lan, W. (2022). Environmental regulation of photosynthetically produced dissolved organic carbon by phytoplankton along a subtropical estuarine bay. *Frontiers in Marine Science*, *9*, 813401. https://doi.org/10.3389/fmars.2022.813401

Kim, B., Kim, S.-H., Kwak, J. H., Kang, C.-K., Lee, S. H., & Hyun, J.-H. (2017). Heterotrophic bacterial production, respiration, and growth efficiency associated with upwelling intensity in the Ulleung Basin, East Sea. *Deep Sea Research Part II: Topical Studies in Oceanography*, *143*, 24–35. https://doi.org/10.1016/j.dsr2.2017.07.002

Kim, B., Kim, S.-H., Min, J.-O., Lee, Y., Jung, J., Kim, T.-W., et al. (2022). Bacterial metabolic response to change in phytoplankton communities and resultant effects on carbon cycles in the Amundsen Sea Polynya, Antarctica. *Frontiers in Marine Science*, *9*, 872052. https://doi.org/10.3389/fmars.2022.872052

Kirchman, D. (2001). Measuring bacterial biomass production and growth rates from leucine incorporation in natural aquatic environments. *Methods in Microbiology*, *30*, 227–237. https://doi.org/10.1016/S0580-9517(01)30047-8

Kujawinski, E. B. (2011). The impact of microbial metabolism on marine dissolved organic matter. *Annual Review of Marine Science*, *3*(1), 567–599. https://doi.org/10.1146/annurev-marine-120308-081003

Lê, S., Josse, J., & Husson, F. (2008). FactoMineR: An R package for multivariate analysis. *Journal of Statistical Software*, *25*, 1–18. https://doi.org/10.18637/jss.v025.i01

Lee, M.-A., Huang, W.-P., Shen, Y.-L., Weng, J.-S., Semedi, B., Wang, Y.-C., & Chan, J.-W. (2021). Long-term observations of interannual and decadal variation of sea surface temperature in the Taiwan Strait. *Journal of Marine Science and Technology*, *29*(4). https://doi.org/10.51400/2709-6998.1587

Liu, H., Browning, T. J., Laws, E. A., Huang, Y., Wang, L., Shang, Y., et al. (2024). Stimulation of small phytoplankton drives enhanced sinking particle formation in a subtropical ocean eddy. *Limnology and Oceanography*, *69*(4), 834–847. https://doi.org/10.1002/lno.12529

Liu, K.-K., Peng, T.-H., Shaw, P.-T., & Shiah, F.-K. (2003). Circulation and biogeochemical processes in the East China Sea and the vicinity of Taiwan: An overview and a brief synthesis. *Deep Sea Research Part II: Topical Studies in Oceanography*, *50*(6–7), 1055–1064. https://doi.org/10.1016/S0967-0645(03)00009-2

Liu, Y., Cai, S., Fan, W., Xiao, W., Liu, X., Laws, E. A., & Huang, B. (2025). Coupling between bacterial phylogenetic diversity and heterotrophic productivity in a coastal ecosystem affected by estuarine plumes. *ISME Communications*, *5*(1), ycaf102. https://doi.org/10.1093/ismeco/ycaf102

Liu, Y., Kang, J., & Huang, Y. (2026). Dataset of primary production and bacterial metabolism in the Taiwan Strait. https://doi.org/10.5281/zenodo.19688915

Lu, Z., Qin, G., Zheng, L., Zhang, Y., Huang, L., Zhou, J., et al. (2025). The role of phytoplankton in structuring global oceanic dissolved organic carbon pools. *Nature Communications*, *16*(1), 7742. https://doi.org/10.1038/s41467-025-63105-x

Mahadevan, A. (2016). The impact of submesoscale physics on primary productivity of plankton. *Annual Review of Marine Science*, *8*(1), 161–184. https://doi.org/10.1146/annurev-marine-010814-015912

Middelboe, M., Søndergaard, M., Letarte, Y., & Borch, N. (1995). Attached and free-living bacteria: Production and polymer hydrolysis during a diatom bloom. *Microbial Ecology*, *29*(3), 231–248. https://doi.org/10.1007/BF00164887

Moran, M. A., Ferrer-González, F. X., Fu, H., Nowinski, B., Olofsson, M., Powers, M. A., et al. (2022). The ocean's labile DOC supply chain. *Limnology and Oceanography*, *67*(5), 1007–1021. https://doi.org/10.1002/lno.12053

Moran, M. A., Kujawinski, E. B., Schroer, W. F., Amin, S. A., Bates, N. R., Bertrand, E. M., et al. (2022). Microbial metabolites in the marine carbon cycle. *Nature Microbiology*, *7*(4), 508–523. https://doi.org/10.1038/s41564-022-01090-3

Mühlenbruch, M., Grossart, H. P., Eigemann, F., & Voss, M. (2018). Mini-review: Phytoplankton-derived polysaccharides in the marine environment and their interactions with heterotrophic bacteria. *Environmental Microbiology*, *20*(8), 2671–2685. https://doi.org/10.1111/1462-2920.14302

Nielsen, E. S. (1952). Use of radio-active carbon ($^{14}C$) for measuring organic production in the sea. *Journal du Consell Consell International pour l'Exploration de la Mer*, *18*(2).

Peterson, B. J. (1980). Aquatic primary productivity and the $^{14}C$-$CO_2$ method: A history of the productivity problem. *Annual Review of Ecology and Systematics*, *11*(1), 359–385. https://doi.org/10.1146/annurev.es.11.110180.002043

Pontiller, B., Martinez-Garcia, S., Joglar, V., Amnebrink, D., Perez-Martinez, C., Gonzalez, J. M., et al. (2022). Rapid bacterioplankton transcription cascades regulate organic matter utilization during phytoplankton bloom progression in a coastal upwelling system. *ISME Journal*, *16*(10), 2360–2372. https://doi.org/10.1038/s41396-022-01273-0

Poulton, A. J., Daniels, C. J., Esposito, M., Humphreys, M. P., Mitchell, E., Ribas-Ribas, M., et al. (2016). Production of dissolved organic carbon by Arctic plankton communities: Responses to elevated carbon dioxide and the availability of light and nutrients. *Deep Sea Research Part II: Topical Studies in Oceanography*, *127*, 60–74. https://doi.org/10.1016/j.dsr2.2016.01.002

Prakash, G., Rajula, G., & Sarma, V. (2024). Role of phytoplankton composition on exudation of dissolved organic carbon in the Bay of Bengal. *Continental Shelf Research*, *279*, 105296. https://doi.org/10.1016/j.csr.2024.105296

Robinson, C. (2008). Heterotrophic bacterial respiration. In *Microbial ecology of the Oceans* (pp. 299–334). Wiley. https://doi.org/10.1002/9780470281840.ch9

Roshan, S., & DeVries, T. (2017). Efficient dissolved organic carbon production and export in the oligotrophic ocean. *Nature Communications*, *8*(1), 2036. https://doi.org/10.1038/s41467-017-02227-3

Sanchez, G. (2013). *PLS path modeling with R*. Trowchez Editions. Retrieved from http://www.gastonsanchez.com/PLSPathModelingwithR.pdf

Siegel, D. A., DeVries, T., Cetinic, I., & Bisson, K. M. (2023). Quantifying the oceans biological pump and its carbon cycle impacts on global scales. *Annual Review of Marine Science*, *15*(1), 329–356. https://doi.org/10.1146/annurev-marine-040722-115226

Tamburini, C., Canals, M., Durrieu de Madron, X., Houpert, L., Lefèvre, D., Martini, S., et al. (2013). Deep-sea bioluminescence blooms after dense water formation at the ocean surface. *PLoS One*, *8*(7), e67523. https://doi.org/10.1371/journal.pone.0067523

Tang, D., Kester, D. R., Ni, I. H., Kawamura, H., & Hong, H. (2002). Upwelling in the Taiwan Strait during the summer monsoon detected by satellite and shipboard measurements. *Remote Sensing of Environment*, *83*(3), 457–471. https://doi.org/10.1016/S0034-4257(02)00062-7

Teira, E., Hernández-Ruiz, M., Barber-Lluch, E., Sobrino, C., Teixeira, I., Álvarez-Salgado, X. A., et al. (2016). Bacterioplankton responses to riverine and atmospheric inputs in a coastal upwelling system (Ría de Vigo, NW Spain). *Marine Ecology Progress Series*, *542*, 39–50. https://doi.org/10.3354/meps11565

Thornton, D. C. (2014). Dissolved organic matter (DOM) release by phytoplankton in the contemporary and future ocean. *European Journal of Phycology*, *49*(1), 20–46. https://doi.org/10.1080/09670262.2013.875596

Yentsch, C. S., & Menzel, D. W. (1963). A method for the determination of phytoplankton chlorophyll and phaeophytin by fluorescence. *Deep-Sea Research and Oceanographic Abstracts*, *10*(3), 221–231. https://doi.org/10.1016/0011-7471(63)90358-9

Zhang, C. (2021). Responses of summer upwelling to recent climate changes in the Taiwan Strait. *Remote Sensing*, *13*(7), 1386. https://doi.org/10.3390/rs13071386

Zhao, Z., Gonsior, M., Schmitt-Kopplin, P., Zhan, Y., Zhang, R., Jiao, N., & Chen, F. (2019). Microbial transformation of virus-induced dissolved organic matter from picocyanobacteria: Coupling of bacterial diversity and DOM chemodiversity. *ISME Journal*, *13*(10), 2551–2565. https://doi.org/10.1038/s41396-019-0449-1

Zhong, Y., Liu, X., Xiao, W., Laws, E. A., Chen, J., Wang, L., et al. (2020). Phytoplankton community patterns in the Taiwan Strait match the characteristics of their realized niches. *Progress in Oceanography*, *186*, 102366. https://doi.org/10.1016/j.pocean.2020.102366